REAL STRUCTURE OF CRYSTALS. GROWTH OF FILMS. NANOCRYSTALS. TIP STRUCTURES

Atomic Force Microscopy Study of Lysozyme Crystallization

I. V. Yaminsky, N. V. Gvozdev, M. I. Sil'nikova, and L. N. Rashkovich

Physics Faculty, Moscow State University, Vorob'evy gory, 119992 Moscow

e-mail: yaminsky@nanoscopy.org

Abstract—Crystallization of lysozyme from solutions has been studied by the atomic force microscopy method. The surface morphology and the growth kinetics of several faces of the orthorhombic and monoclinic modifications of lysozyme crystals are considered. The surface images are obtained at molecular resolution. For the (010) face of orthorhombic lysozyme, the phenomenon of the surface reconstruction is established—doubling of the unit-cell parameter along the *a*-axis. The main growth parameters of lysozyme are determined—the kink density at steps, probabilities of the attachment and detachment of building blocks, the kink and step velocities, and the dependence of the fluctuation in the step position on time. © *2002 MAIK "Nauka/Interperiodica".*

INTRODUCTION

Lysozyme is a protein with a well-known primary structure. It is a comparatively small protein with a molecular mass of about 14000; it consists of 129 amino acid residues forming one polypeptide chain. Tetragonal lysozyme has three water molecules per each amino acid, whereas two other lysozyme modifications have two water molecules per amino acid. A lysozyme molecule in solutions has an almost ellipsoidal shape with dimensions of $2.8 \times 3.2 \times 3.0$ nm [1] and a volume of 2.7×10^{-20} cm^3.

Lysozyme has six crystalline modifications—tetragonal, orthorhombic, monoclinic, trigonal, triclinic, and hexagonal. Crystallographic data for the first three modifications are listed in Table 1. The volume of a lysozyme molecule in an orthorhombic crystal equals 6×10^{-20} cm^3 and, in a monoclinic crystal, 10.7×10^{-20} cm^3. Two projections of an orthorhombic lysozyme structure, which includes about 40% of the solvent (the *ac*-projection and the *ac*-projection constructed in this study by the data of [4]) are shown in Fig. 1.

The tetragonal modification is studied in detail by the atomic force microscopy (AFM) method. The first attempt to study growth of tetragonal lysozyme by AFM was made by Durbin and Carlson [5], who observed the macrostep motion and two-dimensional nucleation on the crystal surface. Radmacher *et al.* used AFM to study adsorption of lysozyme molecules on mica; they also determined Young's modulus for a monomolecular layer (0.5 ± 0.2 GPa) [6]. Konnert *et al.* [7] and Kuznetsov *et al.* [8] managed to attain molecular resolution at the crystal surface. The growth mechanisms of tetragonal lysozyme crystals were also established by AFM [7, 9–11]. The defect formation at the surface of a growing lysozyme crystal was studied in [9, 12–14]. The building blocks of a tetragonal lysozyme crystal were considered by Wiechmann *et al.* [15], who also established that a kink at a step whose rise is equal to one unit-cell parameter (the unit cell containing four molecules) can travel for a distance of 90 nm for 0.08 s, which corresponds to the incorporation into the step of ten tetramers. They also assumed that such a fast tetramer incorporation is possible only if lysozyme molecules form aggregates in the solution which, later, are incorporated as a whole into the kink. Nevertheless, Wiechmann *et al.* [15] did not exclude possible incorporation of monomers and not aggregates into the kink, because, within the measurement time (0.08 s), individual molecules could also quickly fill the kink.

Table 1. Crystallographic data for lysozyme crystals

Symmetry	Sp. gr.	Unit-cell parameters	Z	Reference
Tetragonal	$P4_32_12$	$a = b = 78.73$ Å, $c = 38.56$ Å	8	[2]
Orthorhombic	$P2_12_12_1$	$a = 56.51$ Å, $b = 73.62$ Å, $c = 30.51$ Å	4	[2]
Monoclinic	$P2_1$	$a = 28.0$ Å, $b = 62.5$ Å, $c = 60.9$ Å, $\beta = 90.8°$	4	[3]
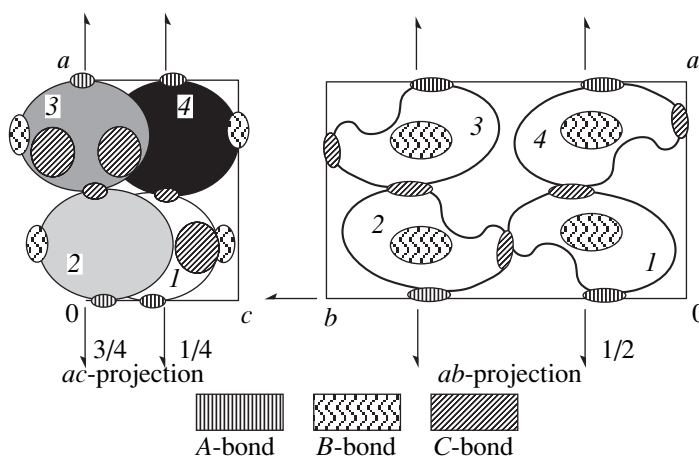
Fig. 1. Molecular packing in an orthorhombic lysozyme crystal. Schematic depiction of the unit cell with macrobonds. On the left, projection in the *ac* plane; on the right, projection in the *ab* plane. For a clearer representation, the molecules are numbered (from *1* to *4*).

Unlike previous works, we studied crystallization of orthorhombic and monoclinic lysozyme modifications. The point is that the formation of several lysozyme modifications under almost equivalent conditions and close temperatures is still unclear. One of the possible explanations for this fact is the formation in the solution of clusters with different dimensions and structures. Upon determination of the size of the kinks attaching building blocks, and, moreover, upon observing these building blocks in an atomic force microscope, one can attempt to verify the above hypothesis. Although we failed to answer this question unambiguously, we managed to reveal a number of other interesting phenomena.

STARTING MATERIALS AND METHODS

The working solutions for the synthesis of orthorhombic and monoclinic lysozyme crystals (5 wt % lysozyme, 5 wt % NaCl, pH 4.6, corrected with the aid of HCl or NaOH and 1 wt % lysozyme, 2 wt % $NaNO_3$ in 50 mM solution of an acetate buffer with pH 4.6, respectively) were prepared from sixfold recrystallized lysozyme (Seikagaku Corp., Japan). We used distilled water with a resistivity of 16 MΩ cm.

Orthorhombic crystals were obtained by the method of spontaneous crystallization as follows. Disklike glass substrates with a diameter of 1 cm and a thickness of 0.5 mm used in the AFM studies were placed into solution thermostated at $t = 40°C$. The substrates were suspended vertically to decrease nucleation. Then the solution temperature was slowly lowered (to avoid mass crystallization) to 35°C. Several hours later, the first crystals appeared on the disks (from several crystals to several dozens of crystals), whose dimensions ranged from dozens of microns to one to two millimeters. In some instances, prior to the formation of the orthorhombic phase, the working solution became tur-

bid because of the formation of a large number of unidentified needlelike crystals. This effect was described in detail elsewhere [16].

Monoclinic lysozyme crystals were obtained in a similar way at room temperature. Later, we also grew lysozyme crystals by the sitting-drop method. With this aim we placed glass substrates on a support into a thermostated vessel in the horizontal position, poured the precipitant into the bottom of the vessel, and applied a droplet of the working solution to the upper surface of each substrate. This method provides growth of large higher quality crystals on the substrates. This method also considerably simplifies the transfer of crystals on the substrates into the growth cell of an atomic force microscope.

During the experiment, supersaturation s was varied by changing the solution temperature, $s = \exp(\Delta\mu/k_BT) - 1 = C/C_0 - 1$, where C and C_0 are the real and equilibrium solution concentrations, k_B is the Boltzmann constant, and $\Delta\mu$ is the chemical potential. The solubility data $C_0(T)$ for orthorhombic and tetragonal crystals in the solutions of the composition used in our experiments within a wide temperature range were taken from [17] and are presented in Fig. 2. As far as we know, there are no data on solubility of monoclinic lysozyme. Since the growth rate of lysozyme in our experiments was rather low, the solution concentration was assumed to be constant, and supersaturation could be varied by changing C_0. To determine the concentration, we took a 100-μl sample from the growth cell and diluted it in 10 ml of 5-wt % NaCl solution. The concentration was determined with the aid of the calibration curve by measuring the optical density of the solution at a wavelength of 281 nm.

The surface morphology of the crystals was studied in a liquid cell of a Nanoscope-3 atomic force microscope in the contact mode. The test measurements in the tapping mode yielded images of much worse quality.

The typical scanning frequency (512 lines) was 10 Hz. When scanning the sample, we maintained the minimum possible tip-sample force to avoid sample destruction. We used commercial Nanoprobe cantilevers (Si_3N_4 tips; mechanical rigidity of the cantilever 0.06–0.38 N/m; gold coated reflecting cantilever surface) and MikroMasch CSC12 cantilevers (Si tips, mechanical rigidity of the cantilever 0.03–0.08 N/m, aluminum coated reflecting cantilever surface). The images obtained with the use of different tips were of the same high quality. Gold-coated cantilevers provided a more pronounced total signal (more reflected light), whereas the aluminum-coated cantilevers provided a higher temperature stability because of a lower thermal bending of the two-layer cantilever.

The data obtained were processed with the use of specialized Femtoscan software (Center of Advanced Technologies, Moscow, Russia).

SURFACE STRUCTURE AT MOLECULAR RESOLUTION

The high-resolution surface image of the (010) face of an orthorhombic lysozyme crystal is shown in Fig. 3. The image is quite typical. To each protrusion, there corresponds one unit cell containing four lysozyme molecules. For this face, two molecules are located on the surface, and two other molecules are located under the former two. The cantilever tip of an atomic force microscope passes around two lysozyme molecules on the surface shown in Fig. 3. Therefore, the image shows not the individual molecules but the protrusions corresponding to these two molecules. The unit-cell dimensions practically coincide with the dimensions obtained by the X-ray diffraction method. It is rather difficult to compare quantitatively the unit-cell dimensions obtained by these two methods because, strictly speaking, a Nanoscope-3 microscope is not a metrological instrument and the accuracy of the corresponding measurements limited by the temperature-induced mechanical drift, nonlinearity, hysteresis, and creep of the ceramic is at a level of 10%.

The image in Fig. 3 was obtained at the minimum possible tip–sample force that can be achieved in a Nanoscope-3 microscope. The estimated value of this force was about 10^{-10} N. The quality images were obtained with the use of both rigid and soft cantilevers, which has a simple explanation. Rigid cantilevers are shorter than soft ones and, therefore, provide a more pronounced deviation of the light beam, which, in the final analysis, can result in a more "delicate" scanning by a cantilever over the surface profile.

Only in some instances did we manage to attain the molecular resolution and obtain the images of individual molecules. We believe that here the main part is played by the cantilever quality, so that only the finest cantilevers can provide the resolution of individual protein molecules.
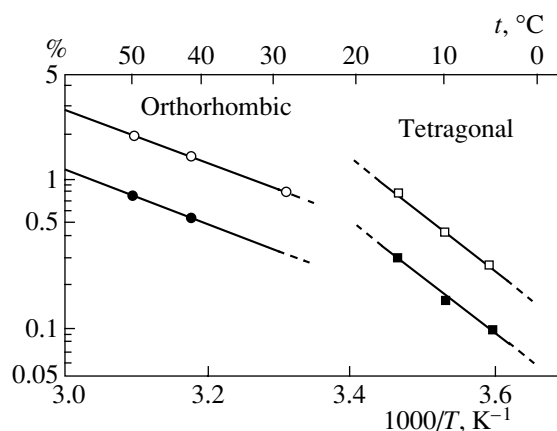
Fig. 2. Solubilities of two crystalline lysozyme modifications as functions of temperature (at pH 4.6). The NaCl content: 3 wt % (light symbols) and 5 wt % (dark symbols).
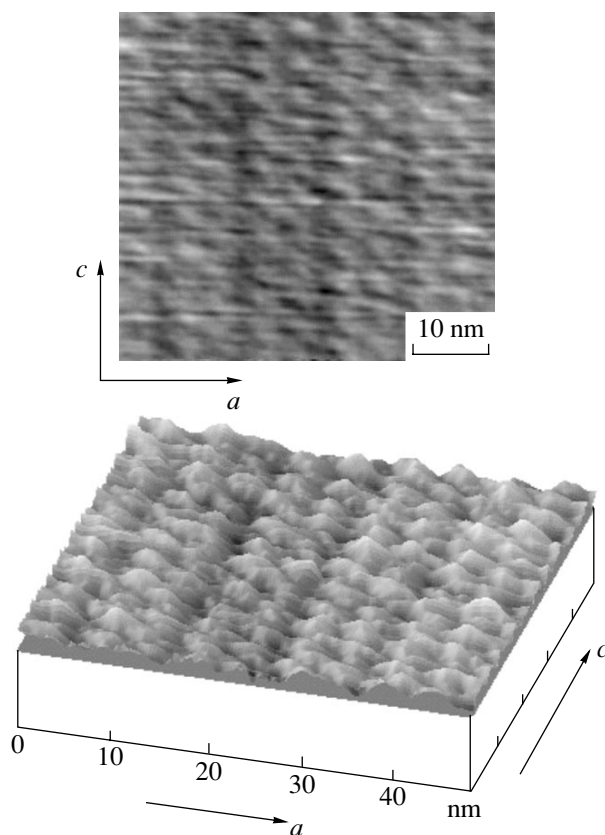
Fig. 3. Doubling of the parameter along the *a* axis on the (010) face of an orthorhombic lysozyme crystal. The original AFM image and its 3D reconstruction.

Doubling of the lattice parameter along the a-axis. If one slightly increases the tip–sample force a during scanning, an interesting phenomenon is observed. The neighboring rows of unit cells oriented along the *c*-axis are seen in the images as protrusions of different heights; the high rows alternate with the low rows. This phenomenon can be interpreted as doubling of the unit-
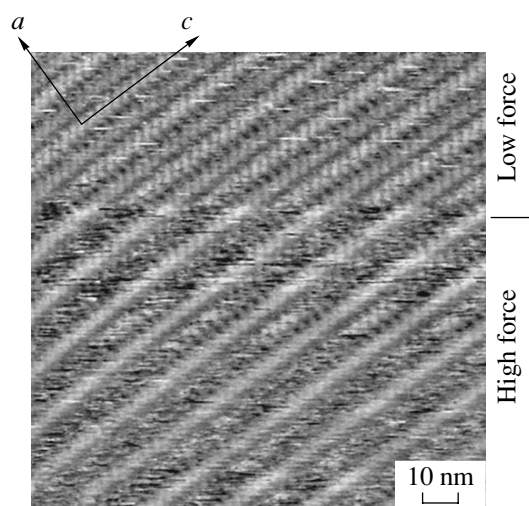
Fig. 4. The image of the regions of the (010) face of an orthorhombic lysozyme crystal at a molecular resolution obtained at different tip–sample forces.
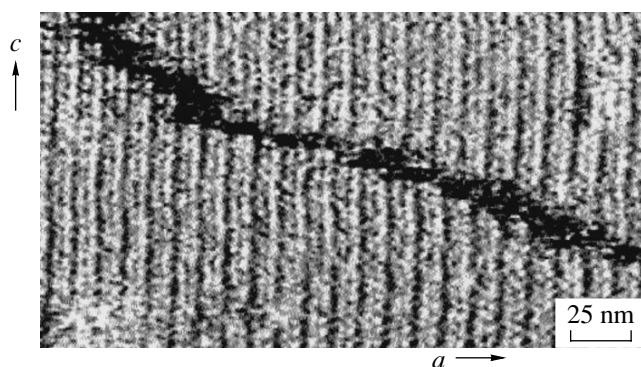
Fig. 5. Image of the region of the (010) face of an orthorhombic lysozyme crystal. The shift of the unit cell in the neighboring growth layers by a half-period. The *b* axis is normal to the drawing plane.

cell parameter along the *a* axis on the surface of the (010) face. Figure 4 shows a surface region at different values of the force applied to the cantilever at a high resolution. This force varied in the process of scanning (in the upward direction). One can clearly see that the neighboring unit-cell rows along the *c* axis are located at different heights ("the region of a high force"). This displacement practically disappears at a slightly lower force ("the region of a low force"). The estimated high force is 1.0×10^{-10} N, and the low force is 0.8×10^{-10} N. Thus, the properties of the neighboring unit cells along the *a* axis are essentially different. This phenomenon can be interpreted as molecule reorientation provided by the unsaturated bonds emerging to the surface. We assumed these bonds to be of *C*-type (Fig. 1). The phenomenon of molecule reorientation on the surface is analogous to the phenomenon of the surface reconstruction well-known for some inorganic materials. The phenomenon of surface reconstruction is, in fact, the process during which the molecules located on the surface are rearranged in comparison with their positions in the crystal bulk in a way that minimizes the free surface energy of the system. This phenomenon was first described for organic crystals in [18] and for tetragonal lysozyme crystals in [19].

In our case, the observed reconstruction depends on the applied force. The difference in the heights of the neighboring unit-cell rows increases with an increase in the force. With a further increase of the applied force, the cantilever seems to strike the molecules from a higher row because of more intense collisions. Indeed, with an increase in the applied force, the higher rows lose the periodicity of their structure and their heights decrease. The image becomes blurred, which can be explained by the "removal" of some protein molecules. Thus, one can draw the conclusion that the neighboring rows have different mechanical rigidity and, therefore, with an increase of the tip–sample force, they are elastically deformed to different degrees.

Doubling of the lattice parameter along the b axis. In neighboring layers in the *ac* plane, the doubled rows of building blocks are shifted by a half-period along the *a* axis, which is well seen if the step is located at an angle to the *c* axis. This situation is shown in Fig. 5 and can be interpreted as doubling of the lattice parameter along the *b* axis, at least, in two surface layers of the building blocks. The measured height of one of these layers equals $b = 7.3 \pm 0.4$ nm.
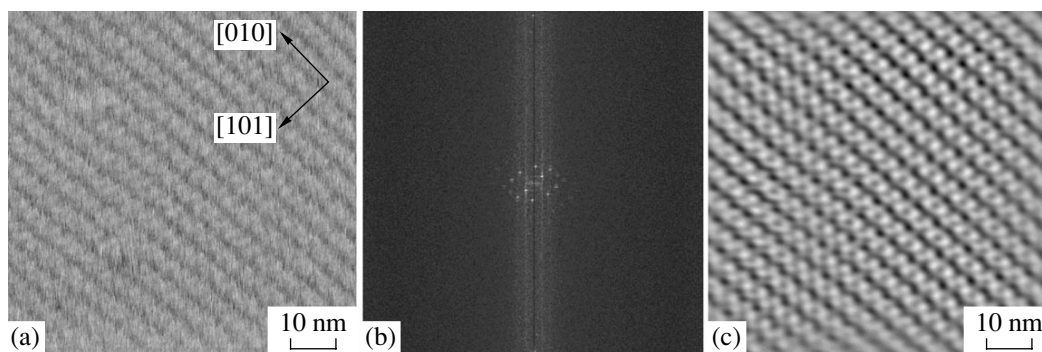
Fig. 6. The surface of a monoclinic lysozyme crystal: (a) initial image, (b) its Fourier transform, and (c) the filtered image.
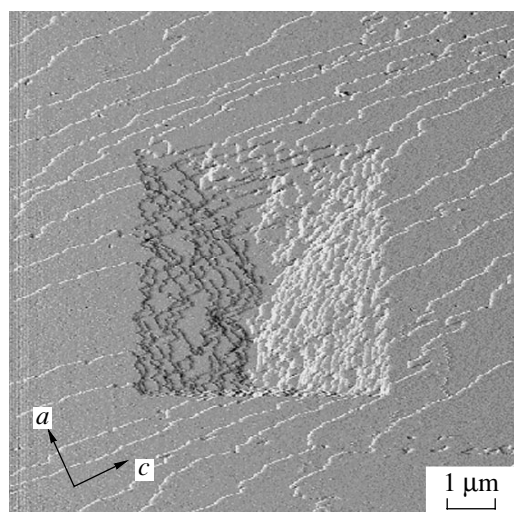
Fig. 7. Depression on the (010) face of an orthorhombic lysozyme crystal formed during long its scanning.

Figure 6 shows the structure of one of the faces of a monoclinic lysozyme crystal. We managed to attain a rather high resolution and visualize the unit cells. The characteristic unit-cell dimensions are 4.6 ± 0.2 nm along the "long" axis of the crystal and 8.5 ± 0.3 nm normal to it. The step rise at this face is 2.6 ± 0.3 nm. No surface reconstruction was observed in this case.

OBSERVATION OF LYSOZYME CRYSTALS SURFACE DESTRUCTION

Scanning in the contact mode at a force lower than 10^{-10} N does not lead to the destruction of the crystal surface. We managed to obtain stable images of a growing face, steps and kinks on this surface, and also the structure of defects. An increase in the force gives rise to the mechanical destruction of the surface including the removal of molecular layers and formation of depressions in the scanned region. Long scanning results in the formation of depressions on the scanned surface area (Fig. 7). The depression bottom formed upon short scanning is flat and has a large number of islands about 7 nm in height (which coincides with the elementary-step rise). With a decrease in the force, the depressions are quickly healed and the crystal face acquires its initial shape.

In some instances, where the force was close to the destruction threshold, the removal of a half-layer was observed. Figure 8a shows the surface region with elementary steps. If a scanning tip moves toward the steps (scanning from right to left), the cantilever "removes" a part of the growth layer and reveals the rougher part of the surface indicated by arrows in Fig. 8. The measured roughness heights showed that the depth of the removed half-layer is equal to the half-height of the growth layer, i.e., $b/2$. Upon the further scanning at a lower force, no destroyed region is seen anymore (Fig. 8b). Unfortunately, it is still unclear why the cantilever removes only a half-cell. It should also be indicated that healing of the damaged surface regions proceeds very quickly (the images in Fig. 8 were taken with an interval of 30 s). Strictly speaking, in this experiment, we did not rigorously control the tip–sample force. The point is that these images were obtained at slow scanning in the upward direction in the first image and in the downward direction in the second image. The different cantilever effect on the surface was caused by a small temperature drift in the downward direction. Also, we cannot exclude a possible effect produced by the tip asymmetry.
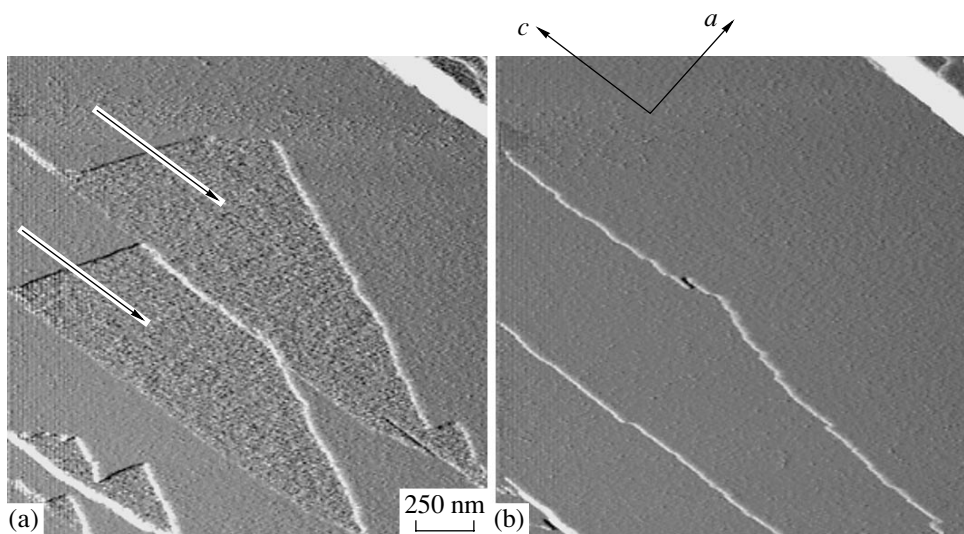
Fig. 8. Region of the surface of the (010) face of an orthorhombic crystal with the elementary steps scanned by the microscope cantilever: (a) scanning in the upward direction; (b) scanning in the downward direction.
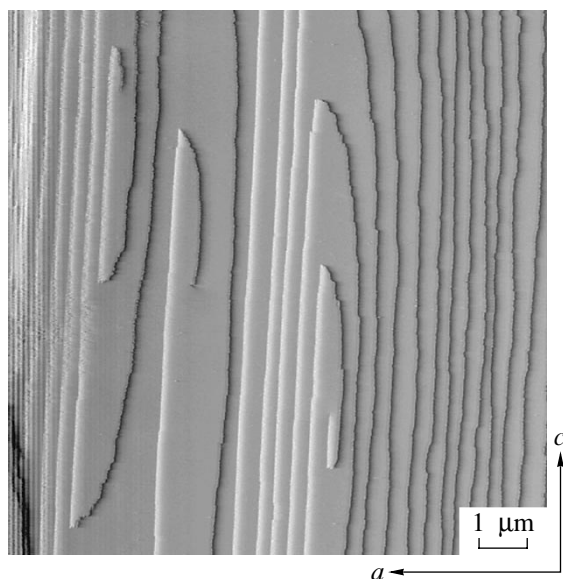
Fig. 9. Dislocation sources on the (010) face of an orthorhombic lysozyme crystal. The *c* axis is directed vertically.
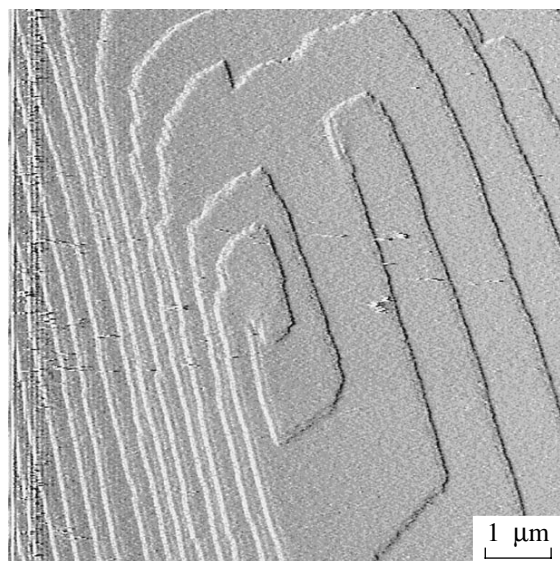
Fig. 10. Two dislocation sources on the face of a monoclinic lysozyme crystal.
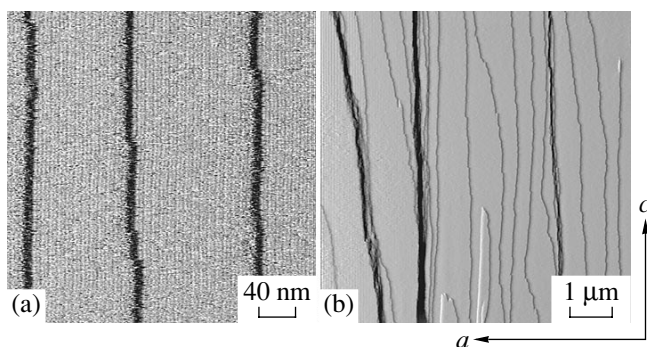
Fig. 11. Images of the surface regions of the (010) face of an orthorhombic crystal with growth steps: (a) elementary steps; (b) elementary steps and their bunching.

SHAPE OF DISLOCATION HILLOCKS

The maximum supersaturation in our experiments was of about 3; however, we observed two-dimensional nucleation in some rare instances. Crystals grew only by the dislocation mechanism. Dislocation hillocks on the (010) face of an orthorhombic lysozyme crystal were somewhat elongated. One of the hillock sides was almost rectilinear and coincided with the *c* axis, whereas the opposite side was bent as an arc and had a pronounced roughness (Fig. 9). The step velocities along the *a* and *c* axes differed by a factor of 7.2.

A dislocation hillock on one of the faces of a monoclinic lysozyme crystal is shown in Fig. 10. Here, the helix is less asymmetric and the ratio of the step velocities along the two perpendicular directions is about 1 : 3. The elementary-step rise equals 2.8 ± 0.3 nm.

OBSERVATION OF MOTION KINETICS OF STEPS AND KINKS

We obtained more than 2000 images of the (010) face of an orthorhombic lysozyme crystal on various scales. The face had both elementary steps and macrosteps. Figure 11a shows the image of the face region containing an echelon of elementary steps with a rise of 7.3 ± 0.4 nm, a value close to the lattice parameter along the *b* axis (Table 1). Figure 11b shows the region of the face not only with elementary steps but also with step bunching (macrosteps). The microstep rise was from two to ten times higher than the elementary-step rise. The velocity of the macrostep motion only slightly differs from the velocity of the elementary steps. Nevertheless, in some instances, the elementary steps caught up with macrosteps and merged into them (step bunching). At the same time, we also observed detachment of elementary steps from the macrostep base. Therefore, the macrostep rise is changed in the process of its motion.

The velocity of an elementary step is practically independent of the interstep distance (0.05–1.00 μm). This is confirmed by the sequence of three images taken with an interval of 50 s shown in Fig. 12. It is seen that the interstep distance is practically constant and, therefore, all the steps move with the same velocity. The steps move from left to right with velocity of about 0.45 nm/s. Therefore, one can conclude that supersaturation for closely located steps is the same as for steps separated by large distances.

We managed to obtain the image of kinks on a moving step at the molecular resolution. The kinks had different depths—from one lattice parameter along the *a* axis (about 80% of kinks) up to four lattice parameters. The existence of kinks only with different depths can be explained by the presence of noncontrolled impurities. The impurity stopper can decelerate the kink only for some time, then the kinks in the following building-block rows can catch up with the stopped kink. However, we have no proof of such a mechanism.
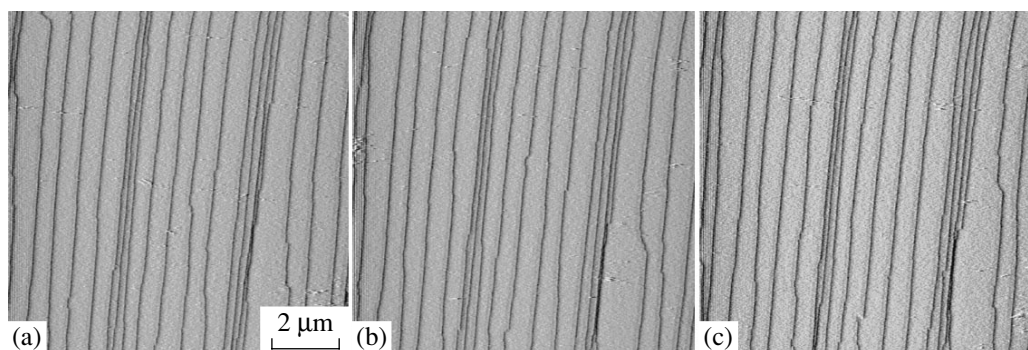
Fig. 12. (a–c) Motion of growth steps on the (010) face of an orthorhombic lysozyme crystal. The images are obtained with an interval of 50 s.

Figure 13 shows a portion of an elementary step with two positive and one negative kink. Their depths are equal to 5.8 ± 0.5 nm, which corresponds to one unit-cell parameter along the a axis. Thus, the kink is formed by four lysozyme molecules. However, the mechanism of kink formation is far from being clear. Possibly, the incorporation of only one molecule gives rise to very quick incorporation of the remaining three molecules. The alternative is the incorporation of a cluster of four molecules.

Concentration of kinks and their velocity. We measured the distances between almost 300 kinks at different steps. The average interkink distance is equal to a dimension comprised of about 180 unit cells, with the root-mean-square deviation being of the same order. The close values of these quantities indicate the exponential distribution function of the interkink distances characteristic of the random distribution of the interparticle distances along the line. The absence of any interaction between the kinks seems to be quite natural at such a low kink density.

At a low kink density, a step moves forward via the formation of rows of building blocks. The arrival of the kink at the given point of the step indicates its motion forward by a distance equal to the dimension of the building block. Therefore, the following relationship is valid:

$$V = b\rho v,$$

where V is the step velocity, v is the kink velocity, ρ is the kink density, and b is the dimension of the building block (the unit-cell parameter) along the direction of step motion. The step velocity can be readily determined from a sequence of its images. The above formula was used to calculate the kink velocity, which turned out to be 100 times higher than the step velocity.

Fluctuations in the step position. Since the building blocks cannot be attached only to the step but can also be detached from it, the step portion moves alternatively forward and backward. In order to observe this process, we switched off the slow-motion mode of the AFM cantilever and scanned only one line. On the step

images of the (110) face thus obtained for orthorhombic lysozyme crystals (Fig. 14); the ordinate axis corresponded to time, the change in the coordinate of the chosen region of the step was measured along the abscissa. The same images can be used to determine the time intervals upon which the building blocks either arrive at or depart from the chosen point of the step. The step coordinate (x^*) as a function of time (t) is shown in Fig. 15. It is seen that, on the average, the step velocity is constant. Subtracting from the x^* values measured at moments t their average value, we arrive at the dependence of the fluctuations in the step position on time $x(t)$. Figure 16 shows the autocorrelation function of this dependence on the logarithmic scale:

$$W^2 = \langle [x(t) - x(t - \Delta t)]^2 \rangle.$$

Here, averaging was performed for all t at the constant Δt. The quantity $W(\Delta t)$ characterizes an increase in the
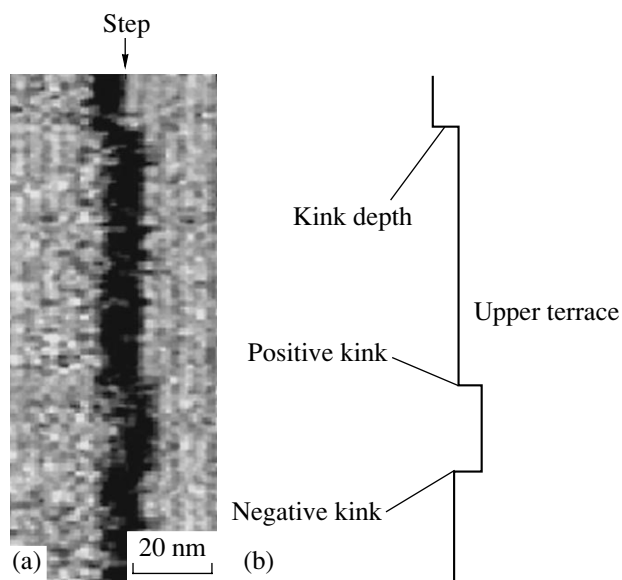
Fig. 13. (a) Portion of an elementary step with two positive and one negative kinks. (a) The step moves from right to left. (b) Schematic depiction of this portion. An orthorhombic lysozyme crystal.
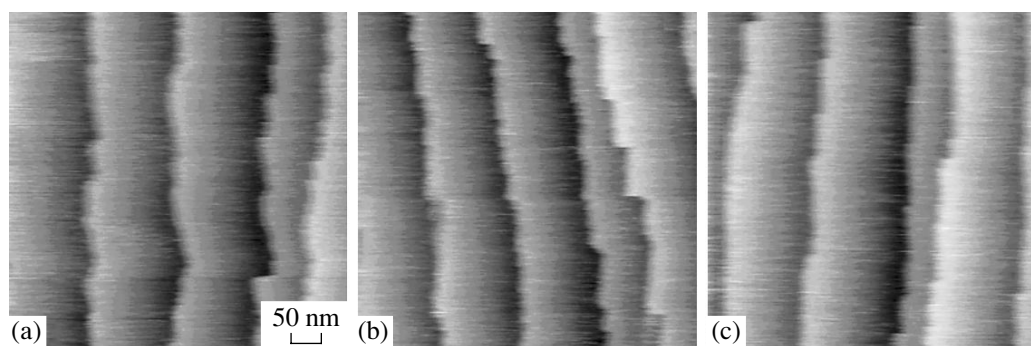
Fig. 14. (a–c) Images of steps on the (110) face of an orthorhombic lysozyme crystal obtained at switched-off scanning along the *y* axis. Scanning time 42 s; cantilever path 512 nm. Scanning frequency 12.2 Hz; scan number 512.
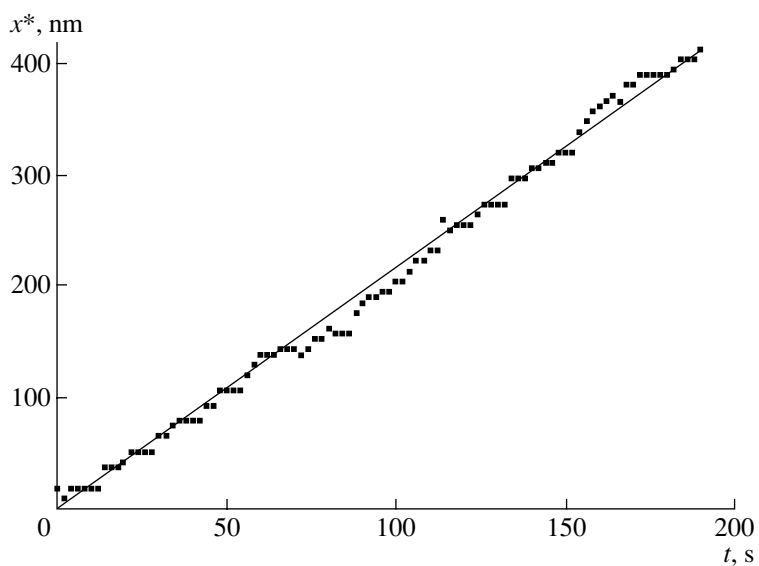
Fig. 15. Coordinate of the step position as a function of time.
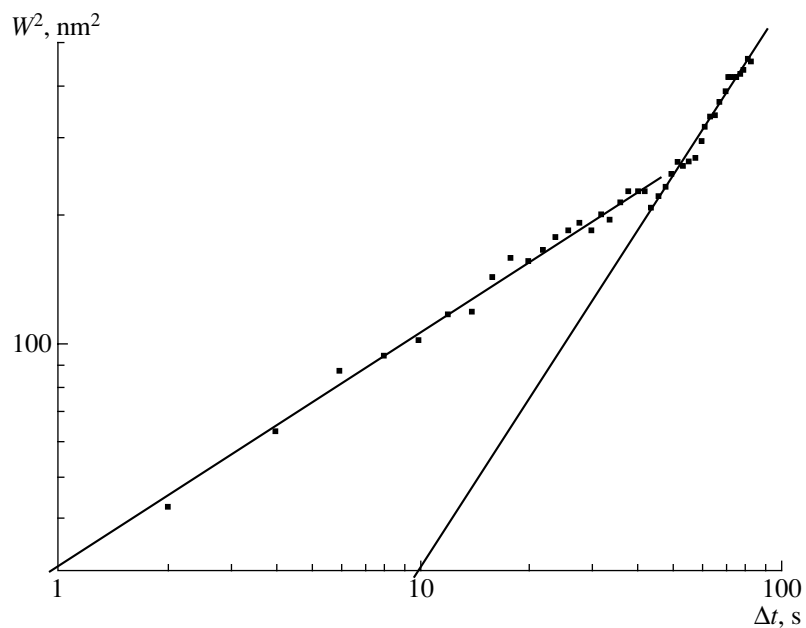
Fig. 16. Autocorrelation function for the dependence *x*(*t*). The curve slope equals 0.53 ± 0.02 nm^2/s for the first region and 1.26 ± 0.04 cm^2/s for the second one.

Table 2. Parameters of lysozyme crystallization calculated from the data on step fluctuations

Parameters	Lysozyme, (110) face, step ∥ [001]
χ, cm^4/s	$(1.22 \pm 0.22) \times 10^{-25}$
a, cm	9.29×10^{-7}
c, cm	3.05×10^{-7}
h, cm	4.48×10^{-7}
$\omega^-(c\rho)^2$, s^{-1}	0.26
β/α_e, cm^2(erg s)	16.1
$c\rho$	0.087
ω^-, s^{-1}	34
β, cm/s	2.86×10^{-6}
α_e, erg/cm	1.71×10^{-7}
α_e/h, erg/cm^2	0.38

intensity of fluctuations (step roughness) for the time Δt. One can see two linear segments. The first one (at small Δt) has a slope equal to 1/2, the second one, 5/4. The second segment of the curve has not been interpreted as yet. However, the first one, which shows that fluctuations increase proportionally to the fourth root of time, confirms the model of the fluctuations in the step position suggested elsewhere [20, 21]. It is assumed in this model that the supersaturation at a step is constant, which agrees with our data that show that the step velocity is independent of the interstep distance. According to [21], we have

$$W^2 = (\chi t)^{1/2},$$

$$\chi = 2(\beta/\alpha_e)kTac/\pi = 2a^4\omega^-(c\rho)^2/\pi,$$

$$\beta = a(c\rho)\omega^-,$$

$$\alpha_e = kTc/(c\rho)a^2.$$

W^2, nm^2
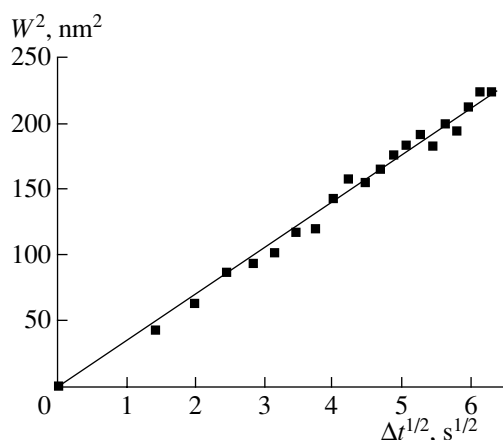
Fig. 17. The first portion of the autocorrelation function in the linearized form.

Here, β is the kinetic coefficient, α_e is the step rigidity, the quantity α_e/h is approximately equal to the free surface energy of the step end (where h is the step rise), k is the Boltzmann constant, T is the temperature, ω^- is the frequency of the detachment of the building blocks from the kinks, and c and a are the distances between the building blocks and their rows, respectively, calculated from the unit-cell dimensions at the given face.

Figure 17 shows the dependence $W^2(\Delta t^{1/2})$, whose slope equals 35.0 ± 0.3 nm^2/s$^{1/2}$ and determines the value of χ. The parameters calculated by the above formulas are listed in Table 2.

The $c\rho$, β, α_e, and ω^- values in the table depend on the building-block dimension. If this dimension differs from the unit-cell dimension, these values can readily be calculated with the use of the experimentally measured χ value.

CONCLUSION

In situ atomic force microscopy provided the study of surface morphology of orthorhombic and monoclinic lysozyme modifications.

A growing crystal face is visualized at molecular resolution. On the (010) face of an orthorhombic lysozyme crystal, the unit-cell parameters are doubled along the a and b axes, which indicates the reconstruction of the surface in the contact with the solution.

Lysozyme crystals grow by the dislocation mechanism, at least at supersaturations $s < 3$. The kinks at the steps, whose density is so low that they cannot interact with one another, are visualized. The steps move via row-by-row filling of the kinks with building blocks. The fluctuations in the positions of the step regions are studied. It is shown that they grow proportionally to the fourth root of time. This is in good accord with the predictions of the theory developed by V.V. Voronkov 30 years ago. The data on fluctuations allowed us to calculate some basic phenomenological and microscopic parameters of crystallization.

REFERENCES

1. L. K. Steinrauf, Acta Crystallogr. **12**, 77 (1959).

2. E. L. Forsythe, E. H. Snell, C. C. Malone, *et al.*, J. Cryst. Growth **196**, 332 (1999).

3. S. T. Rao and M. Sundaralingam, Acta Crystallogr., Sect. D: Biol. Crystallogr. **52**, 170 (1996).

4. H. Oki, Y. Matsuura, H. Komatsu, and A. A. Chernov, Acta Crystallogr., Sect. D: Biol. Crystallogr. **55**, 114 (1999).

5. S. D. Durbin and W. E. Carlson, J. Cryst. Growth **122**, 71 (1992).

6. M. Radmacher, M. Fritz, J. P. Cleveland, *et al.*, Langmuir **10**, 3809 (1994).

7. J. H. Konnert, P. D'Antonio, and K. B. Ward, Acta Crystallogr., Sect. D: Biol. Crystallogr. **50**, 603 (1994).

8. Yu. G. Kuznetsov, A. J. Malkin, T. A. Land, *et al.*, Biophys. J. **72**, 2357 (1997).

9. A. McPherson, A. J. Malkin, and Y. G. Kuznetsov, Structure (London) **3**, 759 (1995).

10. Yu. G. Kuznetsov, A. J. Malkin, W. Glantz, *et al.*, J. Cryst. Growth **168**, 63 (1996).

11. A. J. Malkin, Yu. G. Kuznetsov, and A. McPherson, J. Cryst. Growth **196**, 471 (1999).

12. A. J. Malkin, Yu. G. Kuznetsov, and A. McPherson, J. Struct. Biol. **117**, 124 (1996).

13. Yu. G. Kuznetsov, A. J. Malkin, and A. McPherson, Phys. Rev. B **58**, 6097 (1998).

14. Yu. G. Kuznetsov, A. J. Malkin, and A. McPherson, J. Cryst. Growth **196**, 498 (1999).

15. M. Wiechmann, O. Enders, S. Zeilinger, *et al.*, Ultramicroscopy **86**, 159 (2001).

16. M. Tanaka, M. Yamamoto, K. Kawashima, *et al.*, J. Cryst. Growth **168**, 44 (1996).

17. M. Ataka and M. Asai, J. Cryst. Growth **90**, 86 (1988).

18. A. A. Baker, W. Helbert, J. Sugiyama, *et al.*, J. Struct. Biol. **119**, 129 (1997).

19. H. Li, A. Nadarajah, and M. Pusey, Acta Crystallogr., Sect. D: Biol. Crystallogr. **55**, 1036 (1999).

20. V. V. Voronkov, in *Crystal Growth* (Nauka, Moscow, 1975), Vol. 11, p. 357.

21. V. V. Voronkov, in *Crystals*, Vol. 9: *Modern Theory of Crystal Growth I*, Ed. by A. A. Chernov and H. Müller-Krumbhaar (Springer-Verlag, Berlin, 1983), p. 7.

Translated by L. Man